Applied Physics Letters

RESEARCH ARTICLE | JUNE 12 2024

Terahertz refractometry of hard-to-access objects using the sapphire endoscope suitable for harsh environments

Gleb M. Katyba ; Sergey P. Lebedev; Anna S. Kucheryavenko ; Irina N. Dolganova ; Nikita V. Chernomyrdin ; Maria G. Burdanova ; Igor E. Spektor ; Maksim Skorobogatiy ; Vladimir N. Kurlov ; Kirill I. Zaytsev

Check for updates

Appl. Phys. Lett. 124, 243703 (2024)
https://doi.org/10.1063/5.0207898

View Online
Export Citation

Articles You May Be Interested In

Marine motor oils refractometry

AIP Conf. Proc. (December 2024)

Gas modulation refractometry for high-precision assessment of pressure under non-temperature-stabilized conditions

J. Vac. Sci. Technol. A (April 2018)

Gas equilibration gas modulation refractometry for assessment of pressure with sub-ppm precision

J. Vac. Sci. Technol. B (May 2019)

09 April 2025 16:20:59

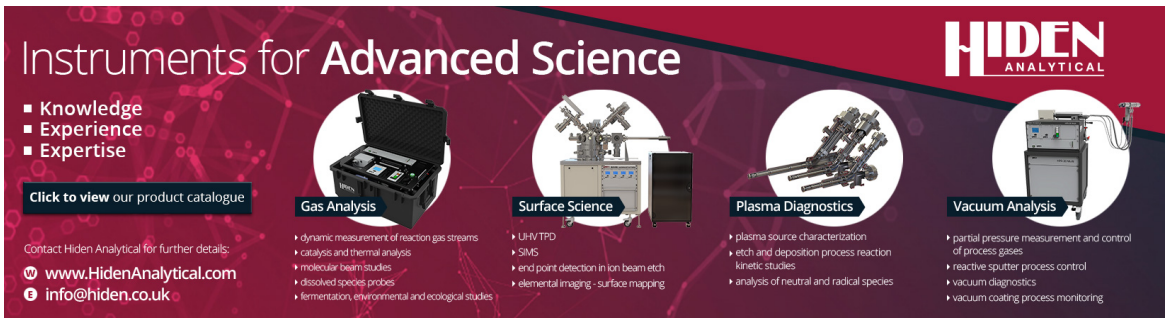

AIP Publishing

Applied Physics Letters ARTICLE pubs.aip.org/aip/apl

Terahertz refractometry of hard-to-access objects using the sapphire endoscope suitable for harsh environments

Cite as: Appl. Phys. Lett. **124**, 243703 (2024); doi: 10.1063/5.0207898
Submitted: 15 April 2024 · Accepted: 29 May 2024 ·
Published Online: 12 June 2024

View Online Export Citation CrossMark

Gleb M. Katyba,[1,a)] Sergey P. Lebedev,[2] Anna S. Kucheryavenko,[1] Irina N. Dolganova,[1] Nikita V. Chernomyrdin,[2] Maria G. Burdanova,[1,3] Igor E. Spektor,[2] Maksim Skorobogatiy,[4] Vladimir N. Kurlov,[1] and Kirill I. Zaytsev[2]

AFFILIATIONS

[1]Osipyan Institute of Solid State Physics of the Russian Academy of Sciences, 142432 Chernogolovka, Russia
[2]Prokhorov General Physics Institute of the Russian Academy of Sciences, 119991 Moscow, Russia
[3]Moscow Center for Advanced Studies, 123592 Moscow, Russia
[4]Department of Engineering Physics, Polytechnique Montréal, Montreal, Quebec H3C 3A7, Canada

[a)]Author to whom correspondence should be addressed: katyba_gm@issp.ac.ru

ABSTRACT

While terahertz (THz) technology offers a variety of applications in medical diagnosis, nondestructive testing, and quality control, its acceptance in these practical fields is hampered by the absence of endoscopic systems, capable of sensing the complex refractive index of the hard-to-access objects. In this paper, we develop the THz endoscope based on the hollow-core antiresonant waveguide, formed by a polytetrafluoroethylene (PTFE)-coated sapphire tube with the outer end closed by a monolithic sapphire window. The endoscope is attached to the backward wave oscillator spectrometer to measure the sample reflectivity. By studying the well-known liquid and solid samples, we demonstrate that analysis of the Fabry–Pérot resonance in the measured reflection spectra makes it possible to quantify the complex refractive index of an analyte. Thanks to the advanced chemical inertness and thermal strength of sapphire and PTFE, the developed endoscope is capable of operation in harsh environments, which broadens the range of its applications. Our findings pave the way for the THz technology use in a number of demanding practical fields.

Published under an exclusive license by AIP Publishing. https://doi.org/10.1063/5.0207898

09 April 2025 16:20:59

Terahertz (THz) technologies have been vigorously explored during the past decades.[1–8] Today, they offer a variety of applications in medical diagnostics,[9] nondestructive testing,[10] quality control,[11] etc. These applications often rely on studies of the THz optical properties of an analyte. Despite THz technologies becoming ubiquitous, its transitioning into such practical fields is hampered by an absence of the THz endoscopes to study hard-to-access objects.[9,12] In fact, in the visible–infrared range, a variety of endoscopic systems exist, allowing to solve modern problems of biomedicine,[13] industrial testing,[14] environmental monitoring,[15] and sensing in harsh environments.[16] In contrast, in the THz range, a lack of such systems is evident, which can be attributed to the nascent state of endoscopy hardware and data processing.[9,17,18]

Within a THz endoscope, an enabling technology is a THz fiber, which was recently developed based on the different material platforms, fabrication strategies, and guiding mechanisms;[17,18] among them: the metal tubes and planar waveguides, which guide THz waves due to their reflections from the metal walls;[19] single or multiple metal wire-based plasmonic waveguides,[20] including the wire medium;[21] step-index dielectric fibers, which use the total internal reflection;[22] and hollow-core waveguides exploiting the antiresonance[23] or photonic crystal[24] guiding mechanisms. While THz waveguiding over considerable distances of meters and larger is still challenging, all the aforementioned waveguides make possible efficient THz delivery at distances of tens of centimeters with appropriate dispersion and loss, making them suitable for endoscopy. Most of them are made of polymers, metals, or both, having limited mechanical strength, chemical inertness, and thermal and radiation resistance, which reduces their capabilities in harsh environments. This drawback was mitigated, to some extent, by using the sapphire shaped crystals produced by the edge-defined film-fed growth (EFG) technique.[18] Indeed, sapphire (α-Al_2O_3) features high refractive index and low absorption at THz

Published under an exclusive license by AIP Publishing

frequencies, together with mechanical and radiation strength, chemical inertness, and biocompatibility; while the EFG technique allows producing tens of centimeter-long optical-quality crystals with complex cross sections, without expensive mechanical processing. In this way, the EFG technique was applied to produce the hollow-core waveguides,[25,26] single optical fibers, and fiber bundles.[27]

To date, only a few waveguides (mostly dielectric) were applied to characterize hard-to-access objects using pulsed or continuous-wave THz radiation.[29–31] Even so, all these fiber-based systems were not used to quantify the THz optical constants, as demanded by the majority of THz applications. That said, many THz waveguides were used for intrawaveguide refractometry, with a focus on sensing small amounts of an analyte introduced into the waveguide.[25,32] An alternative approach to measuring the THz optical constants of a hard-to-access object is to use endoscopes based on either a pair of fiber-coupled THz photoconductive antennas or a fiber-coupled THz transceiver.[33–35] They exploit THz wave generation and detection near an object, while optical fibers are used to flexibly deliver pump and probe laser beams to the THz emitter and detector. While such systems have already been applied to study the THz response of superficial tissues, they remain rare, expensive, and cumbersome. Thereby, THz endoscopy remains challenging and requires further research and engineering efforts.

In this paper, we report the THz endoscope, based on the hollow-core antiresonant sapphire waveguide (Fig. 1). We use the antiresonant guiding mechanism since it provides a compromise between the dimensions of a waveguide core and the dispersion and propagation loss of a guided mode.[9,18] The waveguide is formed by a 50-mm-long sapphire tube with inner and outer diameters of 6.3 and 7.6 mm, respectively. The tube is coated with a 0.4-mm-thick PTFE film and terminated by a monolithic 1.055-mm-thick sapphire window from the side of an object. Together with the in-house backward wave oscillator (BWO) spectrometer, the waveguide is used to measure reflectivity (by power) of different test media, the THz optical properties of which were characterized *a priori* using the in-house transmission-mode THz pulsed spectrometer (TPS). The test media include de-ionized water, pure propylene glycol (PG) and its aqueous solutions, 96% ethanol, glycerol, and gelatin. Since our endoscopic system allows us to measure only the power reflection spectra, it seems like it does not allow us to collect enough information to characterize the complex refractive index of a sample $\tilde{n} = n' - in'' \equiv n - i\frac{c_0}{4\pi\nu}\alpha$, where $n' \equiv n$ is the refractive index, α is the power absorption coefficient, ν is the frequency, and $c_0 \simeq 3 \times 10^8$ m/s is the speed of light in free space. However, instead of using simple refractometry, we resort to studying the Fabry–Pérot resonances excited in the reflection spectra due to the standing waves inside a sapphire window in contact with an analyte. Analysis of the position and the modulation depth of such resonances allows us to quantify both the n- and α-parameters. Studies of a variety of test samples and comparisons of the endoscopic BWO-based estimations of their n and α with the TPS data reveal the high fidelity of the proposed approach. Moreover, thanks to the advanced mechanical, chemical, and thermal performance of the sapphire and PTFE materials used in the endoscope fabrication, we believe that it is capable of operation in harsh environments, which even extends the range of its applications.

In Fig. 1(a), a schematic of the experimental setup is shown. It uses the in-house BWO as a continuous-wave THz emitter with the output frequency tunable in the 0.55–0.715 THz range, the $\sim 10^{-5}\nu$ linewidth, and the $\simeq$1–10 mW output power. The off-axis parabolic mirror with the 50 mm diameter and the 100 mm focal length is used to focus the THz beam on the input end of the endoscope, while a conical diaphragm in front of it minimizes the parasitic reflections and prevents excitation of the higher order modes. The reflected THz signal is detected using the in-house Golay cell with the $\sim 10^{-5}$ V/W sensitivity and the $\sim 10^{-1}$ s time response.

In Fig. 1(b), sapphire tube fabrication via the EFG method is illustrated, while in (c), a photo of the as-grown tube is shown, where the sapphire c-axis is directed along the tube axis. In contrast to single-point, two-point, or tube-shaped seeds applied for the crystal growth initiation in Refs. 18 and 25, here, the 1.055-mm-thick c-cut polished sapphire window is used both as a seed (during the growth process) and as a monolithic flat outer window (during the endoscopy). For the

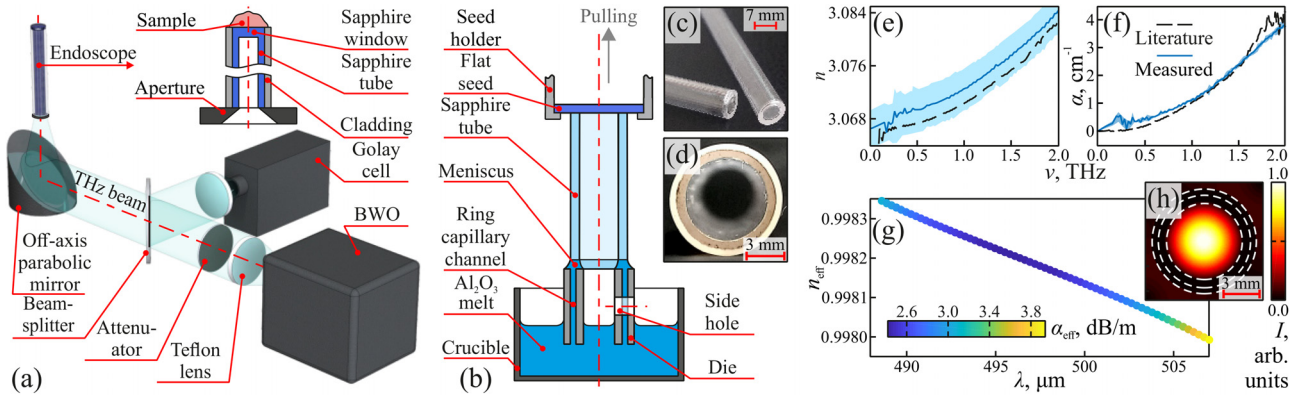

FIG. 1. (a) Schematic of the BWO-based experimental setup for the endoscopic reflectometry, where the insert shows the sapphire endoscope with an integrated window, atop of which a sample is placed. (b) Schematic of the sapphire tube growth using the EFG technique and the c-cut sapphire window as a seed. (c) A photo of the as-grown sapphire tube with a close end (without a polymer coating). (d) A photo of the waveguide cross section (with a polymer coating). (e) and (f) THz optical properties of sapphire for the ordinary ray, measured by TPS and compared with Ref. 28. (g) and (h) Numerical effective refractive index n_{eff} and power loss α_{eff} of the fundamental mode, as well as the its intensity $I(\mathbf{r})$ at $\nu = 0.6$ THz. Panels (d), (g), and (h) are adapted with the permission from Kucheryavenko *et al.*, Opt. Express **31**, 13366 (2023).[26] Copyright 2023 Optica Publishing.

09 April 2025 16:20:59

Published under an exclusive license by AIP Publishing

details of crystal growth, see the supplementary material. The as-gown sapphire tube has the inner and outer diameters of 6.3 and 7.6 mm, respectively, the length of tens of centimeters. After the EFG-growth, a 50-mm-long piece was cut from the tube and coated with a 0.4-mm-thick PTFE film via the thermal polymer shrinkage [Fig. 1(d)].

In Figs. 1(e) and 1(f), we show the THz optical properties of bulk sapphire for the ordinary ray propagating along the *c*-axis, where our TPS data agree with Ref. 28. In Figs. 1(g) and 1(h), we reproduce from Ref. 26 the numerical data for the effective refractive index n_{eff} and propagation loss α_{eff} of the fundamental core-guided mode of our waveguide, as well as its intensity $I(\mathbf{r})$ at $\nu = 0.6$ THz, or $\lambda \simeq 500\,\mu$m (calculated using the finite-difference eigenmode method within the ANSYS Mode software). As a first approximation for the spatial resolution of our endoscope, we can consider modal diameter at the full-width at half-maximum, which is 4.2 mm, or $\sim 8.4\lambda$.

Thus, a fabricated endoscope was attached to the BWO spectrometer [Fig. 1(a)] and applied to measure the power reflectivity of a sample $R_{\text{sample}} = I_{\text{sample}}/I_{\text{mirror}}$, which is a ratio between the sample signal I_{sample} acquired with endoscope (reflected from the sapphire window with a sample atop) to reference I_{mirror} (reflected from the gold mirror at the output end of an equivalent waveguide without a window). The sample spectrum I_{sample} shows an interference pattern caused by the standing waves (Fabry–Pérot resonances) inside the window. The resultant minima spectral positions ν_{min} and the reflectivity values R_{min} are directly related to the complex refractive index $\tilde{n}$ of an analyte.[36]

Consider the reflectivity of a three-layer medium using a plane wave approximation at normal incidence, which is valid as the angular divergence for the THz beam leaving such a waveguide is $< 10°$.[37] When neglecting the radiation loss in the window, the R_{min} and ν_{min} take the following form:[38]

$$R_{\text{min}} = \left|\frac{\tilde{r}_{12} - \tilde{r}_{23}}{1 - \tilde{r}_{12}\tilde{r}_{23}}\right|^2, \quad \nu_{\text{min}} = \frac{c_0}{4dn_2'}\left[\frac{\varphi}{\pi} + (2m+1)\right]. \tag{1}$$

Here, d is the window thickness, $m = 0, \pm 1, \pm 2$ is an integer,

$$\tilde{r}_{12} = \frac{\tilde{n}_{\text{eff}} - \tilde{n}_2}{\tilde{n}_{\text{eff}} + \tilde{n}_2}, \quad \tilde{r}_{23} = \frac{\tilde{n}_2 - \tilde{n}}{\tilde{n}_2 + \tilde{n}} \tag{2}$$

are the Fresnel reflection coefficients (by field), corresponding to the endoscope (air)/window and window/object interfaces,

$$\varphi = \arctan\left(\frac{2n_2'n''}{n_2'^2 - n'^2 - n''^2}\right) \tag{3}$$

is the phase shift at the window/object interface, where $\tilde{n}_{\text{eff}} = n_{\text{eff}}' - in_{\text{eff}}'' \equiv n_{\text{eff}} - i\frac{c_0}{4\pi\nu}\alpha_{\text{eff}}$, $\tilde{n}_2 = n_2' - in_2''$, and $\tilde{n} = n' - in''$ are the complex refractive indices of the core-guided mode, sapphire window [see Figs. 1(e) and 1(f)], and analyte, respectively. It is worth noting that $\tilde{n}_{\text{eff}}$ can be replaced by real unity, as seen from the numerical simulation [Fig. 1(g)]. In this case, $\tilde{r}_{12}$ becomes purely real, while $\tilde{r}_{23}$ remains complex. Using Eqs. (1)–(3), $\tilde{n}$ can be then definitely estimated from the Fabry–Pérot resonance parameters R_{min} and ν_{min}. For the details, see the supplementary material. The applied principle is in stark contrast to the Fabry–Pérot sensors in the visible–infrared range that commonly retrieve only the real refractive index while neglecting the imaginary.[39]

The BWO-based endoscopic system is then applied to study the THz refractive index n and power absorption coefficient α of several organic media, common in biophotonics. Those include the de-ionized liquid water, 96% ethyl alcohol, glycerol, PG, and a solid 15% aqueous solution of gelatin, with *a priori*-known optical properties.[40,41] In the THz range, the aforementioned liquids and their aqueous solutions are used as hyperosmotic agents in the immersion optical clearing of tissue,[40,41] while gelatin is a key component of the tissue mimicking phantoms.[41]

For the endoscopy, de-ionized liquid water, pure PG, or their solutions with the PG volume fraction $C_{\text{PG}} = 0$–100% (their optical properties were studied by TPS in the 0.1–2.5 THz range in Refs. 40 and 43) were prepared by the volume–volume method and an ultrasonic stirrer and placed in a 3D-printed polymer cuvette atop the window [Fig. 2(a)]. The thickness of a liquid column over the window was, at least, a few millimeters, which is much larger than the depth of the THz wave penetration in these substances.[40,41] For each sample, several measurements were carried out to estimate mean n and α values, and their standard deviations. Due to the high hardness and chemical inertness of sapphire, the endoscope geometry and optical performance remain unaltered even after multiple reuses and cleaning procedures.

In Figs. 2(b)–2(e), we show representative examples of the endoscope reflectivity curves for the empty cuvette (bare sapphire window), cuvette filled with water ($C_{\text{PG}} = 0\%$), 50% PG aqueous solution ($C_{\text{PG}} = 50\%$), and pure PG ($C_{\text{PG}} = 100\%$), respectively. The experimental reflectivity spectra clearly show the Fabry–Pérot resonance minima near $\nu_{\text{min}} = 0.6$ THz. Their spectral position ν_{min} and reflectivity value R_{min} vary significantly with the sample optical properties n, α. By analyzing changes in the two Fabry–Pérot resonance parameters $\Delta\nu_{\text{min}}$, ΔR_{min} (as compared to an empty window), we deduced the n and α values for liquids, which were found to match the TPS data closely [Figs. 2(f) and 2(g)]. Also, we note that the measured optical properties are well described by the Bruggeman model,[41] while somewhat lower experimental values are attributed to the bonding of water by PG molecules.

In Fig. 2(h), the n and α values at 0.6 THz of pure water, ethanol, glycerol, PG, and gelatin are retrieved from the endoscopy and TPS, where an excellent correspondence between the two datasets is evident. From this, we conclude that the developed endoscopic system and data processing algorithm allow high fidelity estimation of the THz optical properties of an analyte for a wide range of n and α values, both in strong ($\alpha \sim 100\,\text{cm}^{-1}$) and weak ($\sim 10\,\text{cm}^{-1}$) absorption limits. Some discrepancies between endoscopic and TPS data observed for gelatin and water are attributed to several factors. In fact, the quality of reflection-mode measurements can be affected by the parasitic reflection from different elements of an endoscope, such as the aperture, input waveguide edge, and its holder. Also, inhomogeneities can be present in the gelatin (such as small air bubbles[41]), thus, reducing its THz optical constants.

The developed system and method for endoscopic sensing of the complex refractive index of analytes have strong potential for various THz applications, including medical diagnostics of hard-to-access tissues and internal organs.[9] Nevertheless, to objectively uncover the strengths and weaknesses of this method in such applications, we need to study more realistic objects, such as healthy and pathologically altered tissues, which we postponed to our future work.

For real-world applications, further optimization of the setup and method is in order. The endoscope's outer diameter should be reduced

09 April 2025 16:20:59

Published under an exclusive license by AIP Publishing

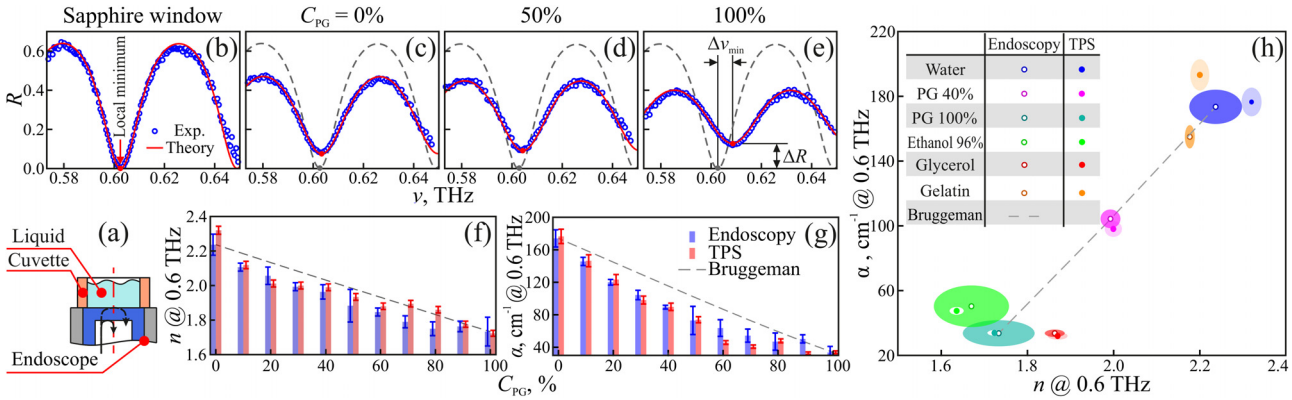

FIG. 2. THz endoscopy of test media with *a priori*-known optical properties. (a) Schematic of the liquid sample measurements in a cuvette, atop the window. (b)–(e) BWO-based reflectivities (by power) of the endoscope in contact with air, water ($C_{PG} = 0\%$), 50% PG solution (by volume, $C_{PG} = 50\%$), and pure PG ($C_{PG} = 100\%$), respectively. To estimate n and α, the experimental data (circles) are fitted by the theoretical model (red solid curve; see the supplementary material), while sample reflectivity is also overlapped with that of an empty window (gray dashed curve). The spectral position ν_{min} and reflectivity value R_{min} for the Fabry–Pérot resonance near $\simeq 0.6$ THz are used to estimate n and α [Eqs. (1)–(3) and the supplementary material]. (f) and (g) The n and α values at 0.6 THz for the PG aqueous solutions with the volume fractions in the $C_{PG} = 0$–100% range, measured by the endoscope, and compared with the TPS data and the Bruggeman model. (h) The n and α values at 0.6 THz for different test samples measured by the endoscopy and compared with the TPS data, where markers stand for the mean values and shaded areas are the $\pm 2\sigma$ confidence intervals. For ethanol, the TPS data are taken from Ref. 42, while for de-ionized water, glycerol, PG, and its aqueous solutions, gelatin, from our earlier works.[40,41]

to $\simeq$3–4 mm, which is preferable for minimally invasive diagnosis and therapy.[9] Considering the selected frequencies, guiding mechanism, and material platform, the outer diameter of such a waveguide can be potentially reduced down to these relevant values. Nevertheless, to produce such a waveguide, the EFG method should be aided by a delicate mechanical processing, aimed at ensuring a high quality ($\sim\lambda/10$) of the waveguide cross section.[44] The endoscope flexibility is desired, which might require resorting to another THz fiber optics material, or guiding mechanism.[9,17,18] For this, the developed method can be adapted for work with the flexible antiresinance[23] or step-index[22] polymer fibers. The dimensions and complexity of the setup can be further reduced, by using a portable diode emitter and a pyroelectric detector of THz waves. The spatial resolution of our endoscope (8.4λ) is enough for some applications, such as sensing of homogeneous tissues or large-scale pathologies (e.g., non-melanoma skin cancers).[9,12] To study a smaller scale pathology (such as dysplastic skin nevi and melanomas) or delineate the tumor margins, the resolution should be improved to 0.1–1.0λ by combining the endoscope with a solid immersion optics.[26] Here, we applied a somewhat impractical calibration procedure that involves rearrangements in the optical path to collect reference and sample signals. A favorable alternative is formed by common calibration and self-calibration methods, used in the reflection-mode spectroscopy with no need for rearrangements.[9,45]

In this paper, we developed the endoscopic Fabry–Pérot sensor to measure the THz complex refractive index of analytes. Our findings justified the efficiency of the developed system and paved the way for the THz remote sensing of hard-to-reach objects.

See the supplementary material for the details of the sapphire tube growth and the inverse problem solution.

The work of G.M.K. and M.G.B. on the design and fabrication of the endoscopic Fabry–Pérot sensor was supported by the Russian Science Foundation (RSF), Project No. 22-72-10033. The work of N.V.C. and K.I.Z. on the experimental study of the endoscopic system was supported by the RSF Project No. 22-79-10099. The work of M.S. on the numerical analysis of the endoscope was supported by the Ubiquitous Terahertz Photonics Project within the Canada Research Chairs Program.

AUTHOR DECLARATIONS

Conflict of Interest

The authors have no conflicts to disclose.

Author Contributions

Gleb M. Katyba: Investigation (equal); Writing – original draft (equal). **Sergey P. Lebedev:** Investigation (equal); Software (equal). **Anna S. Kucheryavenko:** Investigation (equal). **Irina N. Dolganova:** Methodology (equal). **Nikita V. Chernomyrdin:** Methodology (equal). **Maria G. Burdanova:** Methodology (equal). **Igor E. Spektor:** Resources (equal). **Maksim Skorobogatiy:** Investigation (equal); Writing – original draft (equal). **Vladimir N. Kurlov:** Investigation (equal); Methodology (equal). **Kirill I. Zaytsev:** Conceptualization (lead); Supervision (lead); Writing – original draft (lead).

DATA AVAILABILITY

The data that support the findings of this study are available from the corresponding author upon reasonable request.

REFERENCES

[1] H. Guerboukha, K. Nallappan, and M. Skorobogatiy, Adv. Opt. Photonics **10**, 843 (2018).
[2] R. I. Stantchev, D. B. Phillips, P. Hobson, S. M. Hornett, M. J. Padgett, and E. Hendry, Optica **4**, 989 (2017).
[3] V. Cecconi, V. Kumar, J. Bertolotti, L. Peters, A. Cutrona, L. Olivieri, A. Pasquazi, T. J. S. Gongora, and M. Peccianti, ACS Photonics **11**, 362 (2024).

09 April 2025 16:20:59

Published under an exclusive license by AIP Publishing

[4]A. Leontyev, K. Kuznetsov, P. Prudkovskii, D. Safronenkov, and G. Kitaeva, JETP Lett. **114**, 565 (2021).
[5]L. Leibov, A. Ismagilov, V. Zalipaev, B. Nasedkin, Y. Grachev, N. Petrov, and A. Tcypkin, Sci. Rep. **11**, 20071 (2021).
[6]K. Kuznetsov, S. Tarasenko, P. Kovaleva, P. Kuznetsov, D. Lavrukhin, Y. Goncharov, A. Ezhov, D. Ponomarev, and G. Kitaeva, Nanomaterials **12**, 3779 (2022).
[7]M. Koch, D. Mittleman, J. Ornik, and E. Castro-Camus, Nat. Rev. Methods Primers **3**, 48 (2023).
[8]X. Guo, K. Bertling, B. Donose, M. Brunig, A. Cernescu, A. Govyadinov, and A. Rakic, Appl. Phys. Rev. **11**, 021306 (2024).
[9]K. Zaytsev, I. Dolganova, N. Chernomyrdin, G. Katyba, A. Gavdush, O. Cherkasova, G. Komandin, M. Shchedrina, A. Khodan, D. Ponomarev, I. Reshetov, V. Karasik, M. Skorobogatiy, V. Kurlov, and V. Tuchin, J. Opt. **22**, 013001 (2019).
[10]C. Stoik, M. Bohn, and J. Blackshire, Opt. Express **16**, 17039 (2008).
[11]J. Zeitler, P. Taday, D. Newnham, M. Pepper, K. Gordon, and T. Rades, J. Pharm. Pharmacol. **59**, 209 (2010).
[12]H. Lindley-Hatcher, R. I. Stantchev, X. Chen, A. I. Hernandez-Serrano, J. Hardwicke, and E. Pickwell-MacPherson, Appl. Phys. Lett. **118**, 230501 (2021).
[13]G. Keiser, F. Xiong, Y. Cui, and P. Shum, J. Biomed. Opt. **19**, 080902 (2014).
[14]L. Yang, M. Chen, Q. Zhu, T. Yang, C. Wang, and H. Xie, Sens. Actuators, A **296**, 17–23 (2019).
[15]Y. Liu, N. Zhang, P. Li, S. Bi, X. Zhang, S. Chen, and W. Peng, Sens. Actuators, B **301**, 127136 (2019).
[16]H. Chen, M. Buric, P. Ohodnicki, J. Nakano, B. Liu, and B. Chorpening, Appl. Phys. Rev. **5**, 011102 (2018).
[17]M. Islam, C. Cordeiro, M. Franco, J. Sultana, A. Cruz, and D. Abbott, Opt. Express **28**, 16089 (2020).
[18]G. Katyba, K. Zaytsev, I. Dolganova, N. Chernomyrdin, V. Ulitko, S. Rossolenko, I. Shikunova, and V. Kurlov, Prog. Cryst. Growth Charact. Mater. **67**, 100523 (2021).
[19]G. Gallot, S. Jamison, R. McGowan, and D. Grischkowsky, J. Opt. Soc. Am. B **17**, 851 (2000).
[20]Y. Cao, K. Nallappan, G. Xu, and M. Skorobogatiy, Nat. Commun. **13**, 4090 (2022).
[21]C. Simovski, P. Belov, A. Atrashchenko, and Y. Kivshar, Adv. Mater. **24**, 4229 (2012).
[22]K. Nallappan, Y. Cao, G. Xu, H. Guerboukha, C. Nerguizian, and M. Skorobogatiy, Photonics Res. **8**, 1757 (2020).
[23]H. Bao, K. Nielsen, O. Bang, and P. Jepsen, Sci. Rep. **5**, 7620 (2015).
[24]T. Ma, H. Guerboukha, M. Girard, A. Squires, R. Lewis, and M. Skorobogatiy, Adv. Opt. Mater. **4**, 2085 (2016).
[25]G. Katyba, K. Zaytsev, N. Chernomyrdin, I. Shikunova, G. Komandin, V. Anzin, S. Lebedev, I. Spektor, V. Karasik, S. Yurchenko, I. Reshetov, V. Kurlov, and M. Skorobogatiy, Adv. Opt. Mater. **6**, 1800573 (2018).
[26]A. Kucheryavenko, V. Zhelnov, D. Melikyants, N. Chernomyrdin, S. Lebedev, V. Bukin, S. Garnov, V. Kurlov, K. Zaytsev, and G. Katyba, Opt. Express **31**, 13366 (2023).
[27]G. Katyba, M. Skorobogatiy, D. Melikyants, N. Chernomyrdin, A. Perov, E. Yakovlev, I. Dolganova, I. Spektor, V. Tuchin, V. Kurlov, and K. Zaytsev, Phys. Rev. Appl. **18**, 034069 (2022).
[28]D. Grischkowsky, S. Keiding, M. van Exter, and C. Fattinger, J. Opt. Soc. Am. B **7**, 2006 (1990).
[29]P. Doradla, K. Alavi, C. Joseph, and R. Giles, J. Biomed. Opt. **19**, 080501 (2014).
[30]B. You and J.-Y. Lu, Opt. Express **24**, 18013 (2016).
[31]K. Ito, T. Katagiri, and Y. Matsuura, J. Opt. Soc. Am. B **34**, 60 (2017).
[32]A. Kumar, P. Verma, and P. Jindal, J. Opt. Soc. Am. B **38**, F81 (2021).
[33]Y. Ji, E. Lee, S.-H. Kim, J.-H. Son, and T.-I. Jeon, Opt. Express **17**, 17082 (2009).
[34]Y. Chen, S. Huang, and E. Pickwell-MacPherson, Opt. Express **18**, 1177 (2010).
[35]S. Busch, T. Probst, M. Schwerdtfeger, R. Dietz, J. Palaci, and M. Koch, Opt. Express **22**, 16841 (2014).
[36]B. Gorshunov, A. Volkov, I. Spektor, A. Prokhorov, A. Mukhin, M. Dressel, S. Uchida, and A. Loidl, Int. J. Infrared Millimeter Waves **26**, 1217 (2005).
[37]G. Katyba, P. Chizhov, V. Kurlov, I. Dolganova, S. Garnov, K. Zaytsev, and V. Bukin, Opt. Express **30**, 4215 (2022).
[38]M. Born and E. Wolf, *Principles of Optics* (Cambridge University Press, Cambridge, UK, 1999).
[39]Y.-J. Rao, Z.-L. Ran, and Y. Gong, *Fiber-Optic Fabry-Perot Sensors: An Introduction* (CRC Press, Boca Raton, FL, 2017).
[40]G. Musina, I. Dolganova, N. Chernomyrdin, A. Gavdush, V. Ulitko, O. Cherkasova, D. Tuchina, P. Nikitin, A. Alekseeva, N. Bal, G. Komandin, V. Kurlov, V. Tuchin, and K. Zaytsev, J. Biophotonics **13**, e202000297 (2020).
[41]A. Kucheryavenko, I. Dolganova, A. Zhokhov, V. Masalov, G. Musina, V. Tuchin, N. Chernomyrdin, A. Gavdush, D. Il'enkova, S. Garnov, and K. Zaytsev, Phys. Rev. Appl. **20**, 054050 (2023).
[42]P. U. Jepsen, U. Møller, and H. Merbold, Opt. Express **15**, 14717 (2007).
[43]H. Guerboukha, G. Yan, O. Skorobogata, and M. Skorobogatiy, Adv. Opt. Mater. **2**, 1181 (2014).
[44]J.-L. Archambault, R. Black, S. Lacroix, and J. Bures, J. Lightwave Technol. **11**, 416 (1993).
[45]X. Chen and E. Pickwell-MacPherson, APL Photonics **7**, 071101 (2022).

09 April 2025 16:20:59

Published under an exclusive license by AIP Publishing